Optical response and ground state of graphene

T. Stroucken,[1] J. H. Grönqvist,[1,2] and S. W. Koch[1]

[1]*Department of Physics and Material Sciences Center, Philipps University Marburg, Renthof 5, DE-35032 Marburg, Germany*

[2]*Department of Physics, Åbo Akademi University, FL-20500 Turku, Finland*

(Received 1 September 2011; revised manuscript received 27 October 2011; published 21 November 2011)

The optical response and the ground state of graphene and graphene-like systems are determined self-consistently. Deriving equations of motion for the basic variables, graphene Bloch equations are introduced and combined with a variational ansatz. Within the Hartree-Fock approximation, this approach reproduces the gap equation for the ground state. The results show that the Coulomb interaction drastically influences the optical response of graphene and introduces an extremely sensitive dependency on the dielectric environment via static background screening. Regarding the effective fine-structure constant as a control parameter, a transition from a semimetal to an excitonic insulator is predicted as soon as the effective graphene fine-structure constant exceeds a value of roughly 0.5. Above this critical value, the computed optical spectra exhibit a pseudogap and several bright p-like excitonic resonances.

DOI: 10.1103/PhysRevB.84.205445 PACS number(s): 78.67.Wj, 73.22.Pr, 71.35.Lk, 71.30.+h

I. INTRODUCTION

The research interest in graphene has increased dramatically since its first isolation by Geim and co-workers in 2004.[1] In particular, the highly unusual electronic and optical properties have led to a cascade of both theoretical and experimental investigations, exploiting its fundamental underlying physics as well as potential applications in electronic and optoelectronic devices (see Ref. 2 and references therein).

The key for understanding the unique electronic properties of graphene is its exotic band structure that differs substantially from most other condensed matter systems. Based on a tight-binding (TB) model, Wallace predicted in 1947[3] an electronic single-particle spectrum exhibiting two distinct crossing points. In the vicinity of these so-called Dirac points, the dispersion is a cone, similar to the light cone in relativistic mechanics, with the Fermi velocity v_F replacing the speed of light. The occurrence of the cones results from the symmetry between the two equivalent sublattices that build the honeycomb lattice. The sublattice wave functions can be combined into a pseudospinor that then obeys the ultrarelativistic Dirac equation. Hence, from a quantum electro dynamics (QED) point of view, electronic excitations close to the Dirac points of graphene can be considered as charged, massless, chiral fermions. From a condensed matter point of view, as the density of states vanishes at the Dirac points, graphene can be considered either as a semimetal or a vanishing-gap semiconductor.

However, as the TB Hamiltonian neglects many-body interactions completely, the role of the electron-electron Coulomb interaction is still not well understood and still the subject of ongoing research.[4–29] As a convenient measure of the relative importance of the Coulomb interaction, one can use the effective fine-structure constant $\alpha_G = e^2/\epsilon\hbar v_F$, where ϵ is the effective background dielectric constant. For freestanding graphene in vacuum $\alpha_G \approx 2.41$, indicating prominent Coulomb interaction effects.

Generally, one can distinguish between Coulomb modifications of the electronic ground state and Coulombic signatures in the excitation properties. From strongly correlated systems, it is known that the Coulomb interaction can induce a transition from a semimetal to a Mott insulator where, unlike in conventional semiconductors, the gap results from the electron-electron rather than the electron-ion interactions. In particular, the electron exchange interaction has been identified as the dominant mechanism responsible for the opening of a gap.[30]

Methodically, most theoretical treatments of the ground state of a many-body system either use highly simplified model Hamiltonians or they rely on perturbative and/or variational approaches. For graphene, perturbative studies based on a renormalization-group analysis predict a logarithmic divergence of the Fermi velocity, stabilizing the semimetallic ground state.[4–7] However, nonperturbative methods yield a semimetal-to-insulator transition at sufficiently high coupling strengths[8–12] where the predicted critical values for α_G range from 0.5 to 1.5. In particular, the possibility of an excitonic condensate has been explored.[18,20]

From semiconductor physics, it is known that the excitation spectrum in the vicinity of the fundamental band gap is dominated by Coulomb bound electron-hole pairs leading to the appearance of excitonic resonances in the absorption spectra. Mathematically, the excitons obey a hydrogen-like Schrödinger equation, which is commonly referred to as Wannier equation.[31] The exciton binding energy in typical semiconductors is in the range of 1 to 100 meV, i.e., much smaller than the hydrogen ground binding energy. However, bound states exist even in the presence of strong static (background) screening, which preserves the long-range $1/r$ Coulomb tail. In metals, the highly mobile carriers effectively screen this long ranged part of the Coulomb interaction with the consequence that excitonic effects are of minor importance. In graphene, the existence of bound pair states and the importance of screening effects are subjects of current research. Since real massless particles in nature are neutral, the Dirac two-body problem has become a topic of interest only within the graphene research and, until recently, it has not even been clear if bound Dirac pairs exist.[21,32]

Experimentally, an important tool to study microscopic processes in many-body systems is optical spectroscopy, providing information both on the system ground state and the excitation properties. Theoretically, several methods to model the optical response of a quantum mechanical many-body

system are well established, e.g., the density matrix approach, nonequilibrium Green functions, or the systematic cluster expansion approach.[33] In general, these methods rely on the knowledge of the initial state, which is usually the ground state.

In this paper, we extend the microscopic approaches and develop a framework that allows us to determine the ground state and the optical response of graphene and graphene-like systems on the same level of approximation. Our method combines the equations of motion with a variational approach. Within the Hartree-Fock approximation, we obtain gap equations that determine a Bogoliubov ground state.[18,20] With this initial state, we then calculate the linear optical response. The resulting spectra show several bright excitonic resonances below the pseudogap.

The work is organized as follows. In Sec. II, we present the Hamiltonian within the TB approximation. Using this basis, we derive the equations of motion for the dynamical quantities of interest and discuss the role of the Coulomb interaction. Similar equations have been derived previously for carbon nanotubes.[34,35] In Sec. III, we apply the variational principle to the total Hamiltonian and impose the equations of motion as a constraint to obtain a stationary ground state. The resulting gap equations are presented and analyzed numerically. In Sec. IV, we derive the graphene Bloch equations and compute the linear optical response.

II. THE HAMILTONIAN AND EQUATIONS OF MOTION

The system Hamiltonian for a single graphene sheet interacting with a classical light field can be written as

$$\hat{H} = \hat{H}_0 + \hat{H}_I + \hat{H}_C.$$

Here,

$$\hat{H}_0 = \int d^3x\ \hat{\psi}^\dagger(\boldsymbol{x})\left\{\frac{\boldsymbol{p}^2}{2m_0} + \sum_{\boldsymbol{R}_A,\boldsymbol{R}_B} V(\boldsymbol{x}-\boldsymbol{R})\right\}\hat{\psi}(\boldsymbol{x}), \quad (1)$$

describes the motion of the electrons of mass m_0 in the periodic lattice potential, $V(\boldsymbol{x}-\boldsymbol{R})$ is the effective core potential of the carbon atom located at $\boldsymbol{R}$, and $\{\boldsymbol{R}_A\}$ and $\{\boldsymbol{R}_B\}$ are the coordinates of the carbon atoms on each sublattice (See Fig. 1).

$$\hat{H}_C = \frac{1}{2}\int d^3x \int d^3x'\ \hat{\psi}^\dagger(\boldsymbol{x})\hat{\psi}^\dagger(\boldsymbol{x}')V(\boldsymbol{x}-\boldsymbol{x}')\hat{\psi}(\boldsymbol{x}')\hat{\psi}(\boldsymbol{x}) \quad (2)$$

describes the electron-electron interaction via the Coulomb potential $V(\boldsymbol{x}-\boldsymbol{x}') = e^2/\epsilon|\boldsymbol{x}-\boldsymbol{x}'|$, where ϵ is the dielectric constant of the environmental medium.

$$\hat{H}_I = -\frac{e}{2m_0c}\int d^3x\hat{\psi}^\dagger(\boldsymbol{x}) \times\left\{\boldsymbol{p}\cdot\boldsymbol{A}(\boldsymbol{x}) + \boldsymbol{A}(\boldsymbol{x})\cdot\boldsymbol{p} - \frac{e}{c}\boldsymbol{A}^2\right\}\hat{\psi}(x) \quad (3)$$

describes the light-matter interaction within the minimal coupling substitution and $\boldsymbol{A}$ is the vector potential for the optical field.

The interaction Hamiltonian couples the dynamics for the vector potential to the expectation value of the particle current

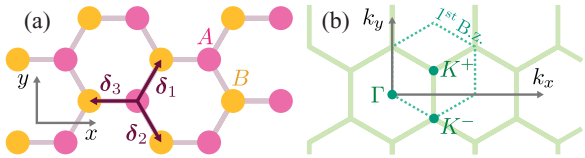

FIG. 1. (Color online) The lattice and the reciprocal lattice.

that can be calculated from the Heisenberg equation of motion,

$$i\hbar\frac{d}{dt}\langle\hat{O}\rangle = \langle[\hat{O},\hat{H}]\rangle + i\hbar\left\langle\frac{\partial}{\partial t}\hat{O}\right\rangle,$$

for the relevant operator $\hat{O}$, yielding a set of coupled differential equations. As is well known, the two-particle Coulomb interaction couples the dynamics for the N-particle expectation values to those of the $(N+1)$-particle expectation values, which is known as the hierarchy problem. In order to achieve a closed set of equations, this hierarchy must be truncated. A systematic truncation scheme is provided by the cluster expansion, which has been proven to work quite well under many different excitation conditions.[33]

In principle, the system dynamics can be described by solving the resulting coupled set of differential equations starting from a predetermined initial state. In a typical experimental setup, the system is excited from the ground state and the response to an externally applied field is measured. Thus, to analyze such experiments theoretically, it is crucial to have an adequate description of the ground state. In semiconductor physics, band structure calculations usually provide a suitable basis to expand the field operators and a good approximation for the ground state. However, this may not be the case in systems where strong carrier-carrier Coulomb interactions influence the ground-state properties.

In the following, we therefore follow an approach where we treat H_0 within the TB approximation and use the resulting eigenfunctions as basis to represent the total Hamiltonian. Within this basis, we then derive the equations of motion on the singlet level, which is equivalent to the time-dependent Hartree-Fock approximation. To determine the ground state on the same level of approximation, we apply the variational approach for the system energy and impose the equations of motion as constraints to guarantee stationarity of the ground state.

A. Tight-binding Hamiltonian

Following the TB approach, we expand the field operators in terms of the carbon wave functions,

$$\begin{aligned}\hat{\psi}(\boldsymbol{x}) &= \frac{1}{\sqrt{N}}\sum_{\boldsymbol{k},\boldsymbol{R}_A} e^{i\boldsymbol{k}\cdot\boldsymbol{R}_A}\phi(\boldsymbol{x}-\boldsymbol{R}_A)\hat{a}_{\boldsymbol{k}} \\ &\quad + \frac{1}{\sqrt{N}}\sum_{\boldsymbol{k},\boldsymbol{R}_B} e^{i\boldsymbol{k}\cdot\boldsymbol{R}_B}\phi(\boldsymbol{x}-\boldsymbol{R}_B)\hat{b}_{\boldsymbol{k}} \\ &= \hat{\psi}_A(\boldsymbol{x}) + \hat{\psi}_B(\boldsymbol{x}). \end{aligned} \quad (4)$$

Here, $\hat{a}_{\boldsymbol{k}}$ ($\hat{b}_{\boldsymbol{k}}$) annihilates a particle in the state $\{\boldsymbol{k}\}$ on the sublattice A (B), $\phi(\boldsymbol{r}) = r\,e^{-r/2d}\cos\vartheta/\sqrt{32\pi d^5}$ is the carbon $2p_z$ orbital responsible for the optical and electronic properties of graphene, and ϑ is the angle between the carbonic

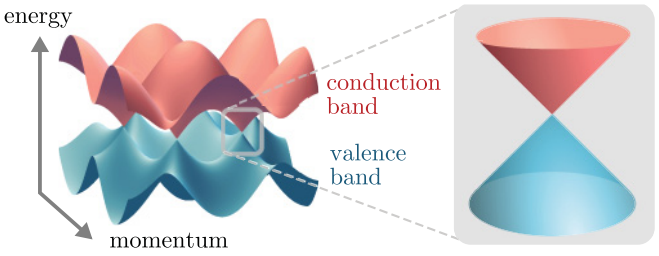

FIG. 2. (Color online) Schematic plot of the π-valence and the π^*-conduction band structure of graphene according to the TB model.

coordinates and the surface normal vector. The parameter $d = a_B/Z_{\text{eff}}$ controls the effective spreading of the carbon wave functions.

Inserting Eq. (4) into the Hamiltonian and taking into account nearest-neighbor hopping only,[36] one obtains for the single-particle part,

$$\hat{H}_0 = \sum_{\boldsymbol{k}} E_F(\hat{a}^\dagger_{\boldsymbol{k}}\hat{a}_{\boldsymbol{k}} + \hat{b}^\dagger_{\boldsymbol{k}}\hat{b}_{\boldsymbol{k}}) + \gamma f(\boldsymbol{k})\hat{a}^\dagger_{\boldsymbol{k}}\hat{b}_{\boldsymbol{k}} + \gamma f^*(\boldsymbol{k})\hat{b}^\dagger_{\boldsymbol{k}}\hat{a}_{\boldsymbol{k}}. \tag{5}$$

Here, E_F is the expectation value of $\hat{H}_0$, γ is the matrix element describing hopping processes between neighboring carbon atoms, $\boldsymbol{\delta}_1 = \frac{a}{2}(1,\sqrt{3})$, $\boldsymbol{\delta}_2 = \frac{a}{2}(1,-\sqrt{3})$, and $\boldsymbol{\delta}_3 = (-a,0)$ are the vectors connecting any carbon atom to its three next neighbors (see Fig. 1), a is the nearest-neighbor distance, and

$$f(\boldsymbol{k}) = \sum_{i=1}^{3} e^{i\boldsymbol{k}\cdot\boldsymbol{\delta}_i}$$

is a function that depends on the lattice symmetry properties only. Diagonalization of $\hat{H}_0$ yields the TB single-particle band structure

$$E^{c/v}_{\boldsymbol{k}} = E_F \pm \gamma|f(\boldsymbol{k})| \tag{6}$$

shown in Fig. 2.

Within the TB approximation, the shape of the bands only depends on the lattice symmetry. The valence and conduction bands are symmetric and touch each other at the two nonequivalent points $\boldsymbol{K}^\pm = (2\pi/3a, \pm 2\pi/3\sqrt{3}a)$ of the Brillouin zone, where the function $f(\boldsymbol{k}) = 0$. Since the ground state of Eq. (5) has a completely filled valence and an empty conduction band, the nodes occur exactly at the Fermi level E_F. In the vicinity of these nodes, a first-order Taylor expansion gives

$$f(\boldsymbol{K}^\pm + \boldsymbol{k}) = -\frac{3a}{2}e^{-i\pi/6}(k_x \pm ik_y).$$

Thus the dispersion is a cone with linear coefficient $3\gamma a/2 \equiv \hbar v_F$, similar to the light cone in relativistic mechanics. Consequently, the electrons behave like massless Dirac fermions with the Fermi velocity replacing the speed of light. Both experimental and theoretical data give a value of approximately 10^6 m/s for the Fermi velocity.

In the following, we will treat $\hat{H}_0$ within the TB approximation. Within the band-structure picture, the Hamiltonian is represented in terms of the electron and hole operators

$$\hat{e}_{\boldsymbol{k}} = \frac{1}{\sqrt{2}}[\hat{a}_{\boldsymbol{k}} + \tilde{f}(\boldsymbol{k})\hat{b}_{\boldsymbol{k}}], \tag{7}$$

$$\hat{h}^\dagger_{-\boldsymbol{k}} = \frac{1}{\sqrt{2}}[-\hat{a}_{\boldsymbol{k}} + \tilde{f}(\boldsymbol{k})\hat{b}_{\boldsymbol{k}}], \tag{8}$$

with $\tilde{f}(\boldsymbol{k}) = f(\boldsymbol{k})/|f(\boldsymbol{k})|$, yielding

$$\hat{H}_0 = \sum_{\boldsymbol{k}} \gamma|f(\boldsymbol{k})|(\hat{e}^\dagger_{\boldsymbol{k}}\hat{e}_{\boldsymbol{k}} + \hat{h}^\dagger_{-\boldsymbol{k}}\hat{h}_{-\boldsymbol{k}}) + \sum_{\boldsymbol{k}} E_F(\hat{e}^\dagger_{\boldsymbol{k}}\hat{e}_{\boldsymbol{k}} - \hat{h}^\dagger_{\boldsymbol{k}}\hat{h}_{\boldsymbol{k}}) + \sum_{\boldsymbol{k}}(E_F - \gamma|f(\boldsymbol{k})|). \tag{9}$$

Here, the second term only contributes if the electron and hole symmetry is broken, e.g., by doping, and the last term represents the energy of the filled valence band. Since this term is constant, it can be omitted. Taking the TB ground state as a reference, the energy with respect to this reference is obtained by normal ordering of the Hamiltonian within the electron-hole picture.

Important Coulomb contributions arise from on-site scattering processes where each electron remains on its specific sublattice, defining the generic matrix element

$$V(\boldsymbol{q}) = \frac{2\pi e^2}{\epsilon q}F(qd)$$

that depends on the momentum transfer only and is given by the 2D bare Coulomb potential modified by the background dielectric constant ϵ and a form factor $F(qd)$. The form factor

$$F(qd) = \int d^3r \int d^3r' e^{i\boldsymbol{q}\cdot(\boldsymbol{\rho}-\boldsymbol{\rho}')}e^{-q|z-z'|}|\phi(\boldsymbol{r})|^2|\phi(\boldsymbol{r}')|^2$$

with $F(0) = 1$ results from the finite extension of the carbonic p_z orbitals perpendicular to the plane and decreases monotonically with q. Hence, the finite value of $d = a_B/Z_{\text{eff}}$ can be interpreted as the effective thickness of the graphene sheet. As an intrinsic length scale, it fixes the graphene energy unit $E_0 = \hbar v_F/d$ and is crucial for obtaining finite values for the exciton binding energy.[32] The Coulomb matrix elements for the processes where at least one electron is scattered from one sublattice to the other are much smaller and vanish exactly at the Dirac points. These will be neglected.

Expanding the field operators in terms of the electron and hole wave functions produces 2^4 different contributions, some of which describe equivalent processes. The ten nonequivalent normally ordered contributions to the Coulomb interaction,

$$H_C = \frac{1}{2}\sum_{\boldsymbol{q}\boldsymbol{k}\boldsymbol{k}'} V^+_{\boldsymbol{k}\boldsymbol{k}'}(\boldsymbol{q})\hat{e}^\dagger_{\boldsymbol{k}+\boldsymbol{q}}\hat{e}^\dagger_{\boldsymbol{k}'-\boldsymbol{q}}\hat{e}_{\boldsymbol{k}'}\hat{e}_{\boldsymbol{k}} + \frac{1}{2}\sum_{\boldsymbol{q}\boldsymbol{k}\boldsymbol{k}'} V^+_{\boldsymbol{k}\boldsymbol{k}'}(\boldsymbol{q})\hat{h}^\dagger_{-\boldsymbol{k}-\boldsymbol{q}}\hat{h}^\dagger_{-\boldsymbol{k}'+\boldsymbol{q}}\hat{h}_{-\boldsymbol{k}'}\hat{h}_{-\boldsymbol{k}} - \sum_{\boldsymbol{q}\boldsymbol{k}\boldsymbol{k}'} V^+_{\boldsymbol{k}\boldsymbol{k}'}(\boldsymbol{q})\hat{e}^\dagger_{\boldsymbol{k}+\boldsymbol{q}}\hat{h}^\dagger_{-\boldsymbol{k}'-\boldsymbol{q}}\hat{h}_{-\boldsymbol{k}'}\hat{e}_{\boldsymbol{k}}$$
$$+ \sum_{\boldsymbol{q}\boldsymbol{k}\boldsymbol{k}'} V^-_{\boldsymbol{k}\boldsymbol{k}'}(\boldsymbol{q})\hat{e}^\dagger_{\boldsymbol{k}+\boldsymbol{q}}\hat{h}^\dagger_{-\boldsymbol{k}}\hat{h}_{-\boldsymbol{k}'+\boldsymbol{q}}\hat{e}_{\boldsymbol{k}'} + \frac{1}{2}\sum_{\boldsymbol{q}\boldsymbol{k}\boldsymbol{k}'} V^-_{\boldsymbol{k}\boldsymbol{k}'}(\boldsymbol{q})\hat{e}^\dagger_{\boldsymbol{k}+\boldsymbol{q}}\hat{e}^\dagger_{\boldsymbol{k}'-\boldsymbol{q}}\hat{h}^\dagger_{-\boldsymbol{k}'}\hat{h}^\dagger_{-\boldsymbol{k}} + \frac{1}{2}\sum_{\boldsymbol{q}\boldsymbol{k}\boldsymbol{k}'} V^-_{\boldsymbol{k}\boldsymbol{k}'}(\boldsymbol{q})\hat{h}_{-\boldsymbol{k}-\boldsymbol{q}}\hat{h}_{-\boldsymbol{k}'+\boldsymbol{q}}\hat{e}_{\boldsymbol{k}'}\hat{e}_{\boldsymbol{k}}$$

$$- \sum_{qkk'} V^{A}_{kk'}(q)\hat{e}^{\dagger}_{k+q}\hat{h}^{\dagger}_{-k'}\hat{e}^{\dagger}_{k'-q}\hat{e}_{k} - \sum_{qkk'} V^{A}_{kk'}(q)\hat{e}^{\dagger}_{k+q}\hat{e}_{k'}\hat{h}_{-k'+q}\hat{e}_{k} + \sum_{qkk'} V^{A}_{kk'}(q)\hat{h}^{\dagger}_{-k}\hat{h}_{-k'+q}\hat{h}_{-k-q}\hat{e}_{k'}$$
$$+ \sum_{qkk'} V^{A}_{kk'}(q)\hat{e}^{\dagger}_{k'-q}\hat{h}^{\dagger}_{-k}\hat{h}^{\dagger}_{-k'}\hat{h}_{-k-q}, \tag{10}$$

have three different matrix elements,

$$V^{\pm}_{kk'}(q) = \tfrac{1}{4}V(q)[1 \pm \tilde{f}^{*}(k+q)\tilde{f}(k)] \times [1 \pm \tilde{f}^{*}(k'-q)\tilde{f}(k'] \tag{11}$$

$$V^{A}_{kk'}(q) = \tfrac{1}{4}V(q)[\tilde{f}^{*}(k+q)\tilde{f}(k) - 1] \times [1 + \tilde{f}^{*}(k'-q)\tilde{f}(k')], \tag{12}$$

that not only depend on the momentum transfer but also on the momenta of the involved scattering particles. Only within the linear approximation, translational invariance is recovered and the matrix elements with $q = k' - k$, relevant for the Hartree-Fock approximation, are given by

$$V^{\pm}(k-k') = \frac{1}{2}V(|k-k'|)[1 \pm \cos(\theta_k - \theta_{k'})], \tag{13}$$

$$V^{A}(k-k') = \pm\frac{i}{2}V(|k-k'|)\sin(\theta_k - \theta_{k'}). \tag{14}$$

The scattering processes characterized by the different matrix elements are schematically presented in Fig. 3. The repulsive electron-electron (e-e) and hole-hole (h-h) and the attractive electron-hole (e-h) scattering where both particles remain in their initial bands are described by V^{+} [see Fig. 3(a)]. The corresponding processes, where both particles change their bands, are described by V^{-} [see Fig. 3(b)]. Both V^{+} and V^{-} are symmetric with respect to $k - k'$ and equal for both Dirac points. Auger processes, where an e-h pair is created

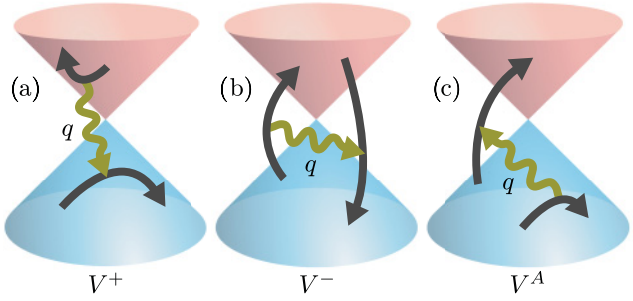

FIG. 3. (Color online) Schematic representation of the Coulomb matrix elements. Figure 3(a) shows the scattering processes where each particle remains in its initial band, described by V^{+}. These processes are a direct generalization of those occurring in wide-gap semiconductors and include the repulsive electron-electron (e-e) and hole-hole (h-h) as well as the attractive electron-hole (e-h) scattering. V^{-} describes processes where both particles change their respective bands, i.e., pair creation or annihilation and scattering of electron-hole pairs under center of mass momentum transfer, shown in Fig. 3(b). Figure 3(c) shows Auger processes, where scattering of a quasiparticle supplies or absorbs the energy and momentum to create or annihilate an e-h pair respectively. The processes shown in Figs. 3(b) and 3(c) require at least one particle to cross the gap and are usually neglected in wide-gap semiconductors.

or annihilated under simultaneous energy and momentum transfer to other quasiparticles, are not ruled out by energy and momentum conservation and are described by the matrix elements V^{A} [see Fig. 3(c)]. These matrix elements are antisymmetric with respect to $k - k'$ and have opposite sign for the two distinct Dirac points. As usual, processes with zero momentum transfer describe a divergent self-interaction that cancels with the electron-ion and ion-ion interaction in the jellium limit and are explicitly subtracted from the Coulomb Hamiltonian.

When computing the optical response, the light-matter interaction is often treated within the dipole approximation. In crystalline solids, this approximation can be obtained by a multipole expansion and subsequent coarse graining over an elementary lattice cell, taking only monopole and dipole contributions into account. In typical direct-gap semiconductors, the distinct symmetry properties of the valence and conduction bands allow us to associate monopole contributions to intraband and dipole contributions to interband transitions, respectively. As inter and intraband transitions involve very different energy scales in a large-gap semiconductor, an optical field couples only to interband transitions, while intraband transitions are in the teraherz range.

In graphene, the situation is quite different. As both the π-valence and π^{*}-conduction bands are constructed from p_z atomic orbitals, they have the same angular momentum quantum numbers and monopole and dipole contributions do not distinguish between different bands. Hence, dipole transitions necessarily involve a superposition of k states required to build a p-like collective state. Additionally, due to the vanishing gap at the Dirac points, inter and intraband transitions take place on the same energy scale.

To derive the correct interaction Hamiltonian, we start from Eq. (3), apply the Coulomb gauge $\nabla \cdot A = 0$, and expand the field operators in terms of the TB wave functions. Making the assumption that the vector potential varies slowly on the length scale of the lattice constant a and sheet thickness d, one finds

$$\hat{H}_I = -\frac{e}{m_0 c}\sum_{k} A \cdot \left(\hbar k - \frac{e}{2c}A\right)(\hat{a}^{\dagger}_{k}\hat{a}_{k} + \hat{b}^{\dagger}_{k}\hat{b}_{k}) - \frac{e}{m_0 c}\sum_{k}[\pi(k)\cdot A\,\hat{a}^{\dagger}_{k}\hat{b}_{k} + \text{H.c.}], \tag{15}$$

where A denotes the field at the position of the graphene sheet, $z = 0$. The first term in the first line of Eq. (15) describes the interaction of the vector potential with the directed current $\hbar k\hat{\rho}_k/m_0$, where $\hat{\rho}_k = -e(\hat{a}^{\dagger}_{k}\hat{a}_{k} + \hat{b}^{\dagger}_{k}\hat{b}_{k})$ is the charge density. This term vanishes because of parity. The second term in the first line of Eq. (15) is proportional to the total electron density n_0 of the π band, yielding a Drude-like response. The

remaining term describes true quantum mechanical transitions, whose strength is determined by the optical matrix element

$$\boldsymbol{\pi}(\boldsymbol{k}) = \sum_i e^{i\boldsymbol{k}\cdot\boldsymbol{\delta}_i} \int d^3x \phi^*(\boldsymbol{r})\boldsymbol{p}\phi(\boldsymbol{r}-\boldsymbol{\delta}_i) = -i\frac{2M}{3a^2}\nabla_{\boldsymbol{k}} f(\boldsymbol{k}) \tag{16}$$

and

$$M = \int d^3x \phi^*(\boldsymbol{r})\boldsymbol{\delta}_i \cdot \boldsymbol{p}\, \phi(\boldsymbol{r}-\boldsymbol{\delta}_i). \tag{17}$$

On-site momentum matrix elements vanish because of parity and hence, in graphene, optical transitions involve inter-sublattice hopping processes. Within the linear approximation, the dipole matrix elements in the vicinity of the Dirac points are given by

$$\boldsymbol{\pi}_\pm(\boldsymbol{k}) = i\frac{\sqrt{2}M}{a} e^{-i\pi/6}\boldsymbol{u}_\pm = -|\boldsymbol{\pi}|e^{-i\pi/6}\boldsymbol{u}_\pm$$

with $\boldsymbol{u}_\pm = (\boldsymbol{e}_x \pm i\boldsymbol{e}_y)/\sqrt{2}$, showing that the two degenerate $\boldsymbol{K}$ points couple to circular polarization components of the optical field.

Transforming the light-matter interaction Hamiltonian into the e-h picture, within the linear approximation, yields

$$\begin{aligned}\hat{H}_I^{[p]} = {} & \frac{e|\boldsymbol{\pi}|}{m_0 c}\sum_{\boldsymbol{k}} A^\pm \cos\theta_{\boldsymbol{k}}(\hat{e}^\dagger_{\boldsymbol{k}}\hat{e}_{\boldsymbol{k}} + \hat{h}^\dagger_{-\boldsymbol{k}}\hat{h}_{-\boldsymbol{k}} - 1) \\ & \pm i\frac{e|\boldsymbol{\pi}|}{m_0 c}\sum_{\boldsymbol{k}} A^\pm \sin\theta_{\boldsymbol{k}}(\hat{e}^\dagger_{\boldsymbol{k}}\hat{h}^\dagger_{-\boldsymbol{k}} - \hat{h}_{-\boldsymbol{k}}\hat{e}_{\boldsymbol{k}}),\end{aligned} \tag{18}$$

where the $\pm$ sign refers to the distinct Dirac points and circular polarization components respectively. Equation (18) clearly shows that optical excitations not only involve interband, but also intraband transitions. Furthermore, the angle dependence in the light-matter Hamiltonian assures that only p-like states couple to an external optical field. Schematic representation of the light-matter interaction is shown in Fig. 4.

B. Equations of motion

In this section, we use the basic single-particle expectation values

$$f_{\boldsymbol{k}} = \langle\hat{e}^\dagger_{\boldsymbol{k}}\hat{e}_{\boldsymbol{k}}\rangle = \langle\hat{h}^\dagger_{-\boldsymbol{k}}\hat{h}_{-\boldsymbol{k}}\rangle, \quad P_{\boldsymbol{k}} = \langle\hat{h}_{-\boldsymbol{k}}\hat{e}_{\boldsymbol{k}}\rangle, \tag{19}$$

as dynamical variables and derive their equations of motion within the time-dependent Hartree-Fock approximation. Due to the band symmetry, the electron and hole populations are

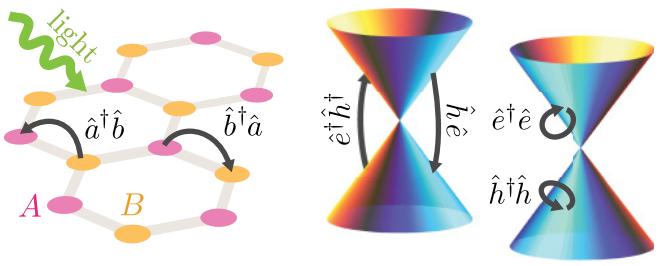

FIG. 4. (Color online) Schematic representation of the light-matter interaction.

equal. Furthermore, as the two equations of motion for the two distinct $\boldsymbol{K}$ points are related by the parity transformation $\boldsymbol{k} \to -\boldsymbol{k}$, $A^\pm \to A^\mp$, we restrict our discussion to a single Dirac point.

Evaluating the commutators in the Heisenberg equations of motion, we obtain the closed set of differential equations

$$i\hbar\frac{d}{dt}P_{\boldsymbol{k}} = 2\Sigma_{\boldsymbol{k}}P_{\boldsymbol{k}} - (1-2f_{\boldsymbol{k}})\Omega_{\boldsymbol{k}} - i\hbar\frac{d}{dt}P_{\boldsymbol{k}}\Big|_{\text{coll}}, \tag{20}$$

$$\hbar\frac{d}{dt}f_{\boldsymbol{k}} = -2\,\text{Im}[P^*_{\boldsymbol{k}}\Omega_{\boldsymbol{k}}] - \hbar\frac{d}{dt}f_{\boldsymbol{k}}\Big|_{\text{coll}}. \tag{21}$$

Here, we introduced the notation

$$\begin{aligned}\Sigma_{\boldsymbol{k}} = {} & \hbar v_F k - \sum_{\boldsymbol{k}'}[V^+(\boldsymbol{k}-\boldsymbol{k}') - V^-(\boldsymbol{k}-\boldsymbol{k}')]f_{\boldsymbol{k}'} \\ & - i\sum_{\boldsymbol{k}'} V^A(\boldsymbol{k}-\boldsymbol{k}')\,\text{Im}P_{\boldsymbol{k}'} + \frac{e|\boldsymbol{\pi}|}{m_0 c}A^\pm\cos\theta_{\boldsymbol{k}} \\ \equiv {} & \Sigma^r_{\boldsymbol{k}}[f_{\boldsymbol{k}}] + \Delta\Sigma_{\boldsymbol{k}}[P_{\boldsymbol{k}}, P^*_{\boldsymbol{k}}, A],\end{aligned} \tag{22}$$

$$\begin{aligned}\Omega_{\boldsymbol{k}} = {} & \sum_{\boldsymbol{k}'} V^+(\boldsymbol{k}-\boldsymbol{k}')P_{\boldsymbol{k}'} + V^-(\boldsymbol{k}-\boldsymbol{k}')P^*_{\boldsymbol{k}'} \\ & \mp i\frac{e|\boldsymbol{\pi}|}{m_0 c}A^\pm\sin\theta_{\boldsymbol{k}} - 2\sum_{\boldsymbol{k}'} V^A(\boldsymbol{k}-\boldsymbol{k}')f_{\boldsymbol{k}'} \\ \equiv {} & \Omega^R_{\boldsymbol{k}}[P_{\boldsymbol{k}}, P^*_{\boldsymbol{k}}, A] - i\Delta\Omega_{\boldsymbol{k}}[f_{\boldsymbol{k}}].\end{aligned} \tag{23}$$

In Eqs. (20) and (21), the terms $d/dt|_{\text{coll}}$ refer to incoherent scattering contributions beyond the Hartree-Fock approximation. To solve the coupled equations, we have to supply the appropriate initial and boundary conditions.

The generalized Rabi energy $\Omega_{\boldsymbol{k}}$ consists of two contributions. $\Omega^R_{\boldsymbol{k}}$ contains the optical field and the internal field of the polarization $P_{\boldsymbol{k}}$ and differs from the standard Rabi frequency known from semiconductors only by the anisotropy resulting from the chiral nature of the Dirac electrons. The additional part $\Delta\Omega$ contains contributions from the populations $f_{\boldsymbol{k}}$ via the Auger processes. Similarly, the generalized renormalized energy $\Sigma_{\boldsymbol{k}}$ has not only terms due to the populations contained in Σ^r, but also Auger contributions from the polarizations and an energy renormalization due to the external field in $\Delta\Sigma_{\boldsymbol{k}}$. For large gap semiconductors, these contributions can be neglected because of energy and momentum conservation. However, for systems with small or vanishing gap, as in graphene, the basic quantities f and P are inherently mixed due to the Auger terms.

Close to the $\boldsymbol{K}^\pm$ point, the Auger contributions to Ω and Σ can be written as

$$\Delta\Omega_{\boldsymbol{k}} = \pm\sum_{\boldsymbol{k}'} V(\boldsymbol{k}-\boldsymbol{k}')\sin(\theta_{\boldsymbol{k}} - \theta_{\boldsymbol{k}'})f_{\boldsymbol{k}'},$$

$$\Delta\Sigma_{\boldsymbol{k}} = \pm\sum_{\boldsymbol{k}'} V(\boldsymbol{k}-\boldsymbol{k}')\sin(\theta_{\boldsymbol{k}} - \theta_{\boldsymbol{k}'})\,\text{Im}P_{\boldsymbol{k}'},$$

respectively. For isotropic densities f and P, the angle integration will give zero and the Auger contributions vanish. The light-matter terms, however, are in themselves anisotropic. The light will therefore excite angular-dependent densities for which the Auger contributions are finite.

In semiconductor physics, the transverse optical field directly only couples to the nondiagonal expectation values P and P^*, which physically represents an optical polarization that can be probed experimentally via optical spectroscopy. Unlike in graphene, the diagonal populations f_k affect optical semiconductor spectra only indirectly through their coupling to the polarization in the semiconductor Bloch equations (SBE).[31] As the linear coupling to the optical field results in a radiative decay of any macroscopic polarization on a picosecond time scale,[37] a (meta)stable initial state may be prepared to contain incoherent diagonal populations but no macroscopic polarizations. In particular, choosing the initial $f_k = 0$ models excitation from the ground state. Expanding the solution of the SBE into powers of the exciting fields gives the well-known series that contains only the odd powers for the polarization and the even powers of the optical field for the populations.[38] Hence, for weak optical fields, the equations for the polarizations and populations can be solved iteratively. The homogeneous part of the polarization equation produces the generalized Wannier equation with the Pauli blocking prefactor $(1 - 2f)$. This homogeneous part is responsible for the formation of bound excitons at low densities, which appear as resonances of the excited system, energetically below the band gap. Inserting increasing amounts of incoherent initial populations leads to a gradual bleaching of excitonic resonances in the absorption spectra and finally produces gain once inversion is reached.

A similar behavior might be expected for the case of graphene. However, the interpretation of the single-particle energy renormalization as "band-edge" renormalization is problematic in a gapless system. Also, bound-exciton solutions of the Wannier equation would predict resonances at negative energies, which is clearly unphysical. This pathological behavior would show up for any incoherent initial population that allows for bound-state solutions of the generalized Wannier equation. Consequently, such a population cannot correspond to a physically meaningful initial state of the system.

In particular, if the linear Wannier equation

$$2\hbar v_F k\,\phi_{\lambda k} - \sum_{k'}[V^+(k-k')\phi_{\lambda k'} + V^-(k-k')\phi^*_{\lambda k'}] = E_\lambda\,\phi_{\lambda k} \tag{24}$$

has bound-state solutions, the TB ground state with $f_k = P_k = 0$ cannot correspond to the ground state of the Coulomb-interacting system. The linear Wannier equation has been analyzed in Ref. 32. Here, it has been shown that bound-state solutions indeed exist for an effective graphene fine-structure constant exceeding the critical value $\alpha_G \approx 0.5$. Below this value, the Coulomb interaction is too weak to create bound states. In this weakly interacting regime, Eqs. (20) and (21) can be solved directly to obtain the optical response and the TB Dirac sea can serve as the ground state of the system. In the regime with strong Coulomb interactions, Eqs. (20) and (21) are not the true graphene Bloch equations, since they do not describe the optical response defined with respect to the correct many-body ground state.

III. GROUND STATE

A. Derivation of the gap equations

A convenient method to determine the ground state is provided by the variational principle

$$\delta\langle\hat{H}\rangle|_{A=0} = 0, \tag{25}$$

where $\delta\langle\hat{H}\rangle|_{A=0}$ is the expectation value of the total energy in the absence of external fields. Due to the Coulomb interaction, the expectation value of the Hamiltonian contains the same many-body correlations as the Heisenberg equations of motion and cannot be solved exactly. To be consistent with the equations of motion, we express the energy expectation value in terms of the same variables as the equation of motion. Within the mean field approximation, these are f_k, P_k and P_k^*, yielding the variational equation

$$0 = \sum_k (2\bar{\Sigma}_k \delta\bar{f}_k - \bar{\Omega}_k^* \delta\bar{P}_k - \bar{\Omega}_k \delta\bar{P}_k^*), \tag{26}$$

where barred quantities refer to ground-state expectation values. However, the dynamic variables are coupled and thus cannot be varied independently of each other.

In order to be radiatively stable, the macroscopic current associated with the ground state must vanish. This condition is fulfilled for all isotropic distributions $\bar{f}_k$ and $\bar{P}_k$. Due to this isotropy, the related Auger contributions to $\bar{\Sigma}_k$ and $\bar{\Omega}_k$ vanish. Furthermore, the ground state clearly has to be a stationary state. Therefore the expectation value of any operator in this state has to be static, such that the time derivative of the basic variables has to vanish. Thus we impose the stationary solution of the equations of motion as constraints to assure a steady state:

$$0 = 2\bar{\Sigma}_k \bar{P}_k - (1 - 2\bar{f}_k)\bar{\Omega}_k, \tag{27}$$

$$0 = -2\,\mathrm{Im}[\bar{P}_k^* \bar{\Omega}_k]. \tag{28}$$

Equation (27) defines the possible distributions for the nondiagonal populations $\bar{P}_k$ in the presence of a given isotropic diagonal population $\bar{f}_k$ subject to the condition that $\bar{P}_k$ is real, imposed by Eq. (28). In itself, the set of Eqs. (27) and (28) puts no constraints on the populations. As the set of Eqs. (27) and (28) always has the trivial solution $P_k = 0$, *any* isotropic carrier distribution defines at least one stable equilibrium state with an associated real polarization defined by Eq. (27). Among these equilibrium states, the ground state minimizes the total energy and can be determined by inserting Eq. (27) into the variational equation. This yields the condition

$$\delta\left[\bar{f}_k(1 - \bar{f}_k) - \bar{P}_k^2\right] = 0 \tag{29}$$

relating $\bar{f}$ and $\bar{P}$. Assuming that the interacting ground state can be generated adiabatically from the noninteracting TB ground state with $f_k = P_k = 0$, the combination of the conditional relation and Eq. (27) allows us to express the ground-state populations in terms of the renormalized energies

and Rabi energies:

$$\bar{P}_k = \frac{1}{2}\frac{\bar{\Omega}_k}{\sqrt{\bar{\Sigma}_k^2 + \bar{\Omega}_k^2}}, \tag{30}$$

$$\bar{f}_k = \frac{1}{2}\left(1 - \frac{\bar{\Sigma}_k}{\sqrt{\bar{\Sigma}_k^2 + \bar{\Omega}_k^2}}\right). \tag{31}$$

Inserting these into Eqs. (22) and (23) yields the coupled set of integral equations

$$\bar{\Omega}_k = \frac{1}{2}\sum_{k'} V(\boldsymbol{k}-\boldsymbol{k}')\frac{\bar{\Omega}_{k'}}{\sqrt{\bar{\Sigma}_{k'}^2 + \bar{\Omega}_{k'}^2}}, \tag{32}$$

$$\bar{\Sigma}_k = \hbar v_F k - \frac{1}{2}\sum_{k'} V(\boldsymbol{k}-\boldsymbol{k}') \times \cos(\theta_k - \theta_{k'})\left(1 - \frac{\bar{\Sigma}_{k'}}{\sqrt{\bar{\Sigma}_{k'}^2 + \bar{\Omega}_{k'}^2}}\right), \tag{33}$$

from which the renormalized and Rabi energies may be calculated numerically. The set of Eqs. (32) and (33) are equivalent to those derived in Ref. 18 and combine the so-called gap equation for $\bar{\Omega}_k$ and the equation for the renormalized single-particle energy $\bar{\Sigma}_k$.

The set of Eqs. (30)–(33) displays several interesting features. From Eq. (31), one recognizes that $\bar{f}_k > 1/2$ implies a negative renormalized energy $\bar{\Sigma}_k < 0$ and $\bar{f}_k < 1/2$ implies $\bar{\Sigma}_k > 0$, respectively. From Eqs. (32) and (33), we notice the properties $\bar{\Omega}_k > 0$ for any nontrivial solution of Eq. (32) and $\bar{\Sigma}_{k=0} = 0$ for any isotropic particle distribution, the latter relation resulting from angle integration. Hence, for any nontrivial isotropic solution of the gap equation one has $\bar{f}_{k=0} = \bar{P}_{k=0} = 1/2$, i.e., the electrons are in a state that mixes the tight-binding valence and conduction bands with equal probability.

In general, the solution of the gap equation is not unique. This reflects the fact that the many-body Hamiltonian may have more than one stationary mean-field solutions fulfilling the variational condition (26). In particular, the gap equation (32) always has the trivial solution $\bar{\Omega}_k = \bar{P}_k = 0$, corresponding to a completely incoherent state. For the incoherent state, Eq. (31) simplifies to $\bar{\Sigma}_k = \hbar v_F k - \sum_{k'}^{k_F} V(\boldsymbol{k}-\boldsymbol{k}')\cos(\theta_k - \theta_{k'})$ with $\bar{f}_k = [1 - \mathrm{sg}(\bar{\Sigma}_k)]/2 = \theta(k_F - k)$ and $\bar{\Sigma}_{k_F} = 0$ fixes the Fermi wave number k_F. Hence, as $\Sigma_{k=0} = 0$, the tight-binding ground state always solves the gap equation and hence corresponds to a stationary mean-field solution of the many-body Hamiltonian, though not necessarily the ground state.

B. Properties of the ground state

To achieve intuitive insight into the nature of the ground state and to derive a criterion for the existence of a nontrivial solution of the gap equation, we implement the conditional relation (29) via

$$\bar{f}_k = \frac{\beta^2\phi^2(\boldsymbol{k})}{1 + \beta^2\phi^2(\boldsymbol{k})}, \tag{34}$$

$$\bar{P}_k = \frac{\beta\phi(\boldsymbol{k})}{1 + \beta^2\phi^2(\boldsymbol{k})^2}. \tag{35}$$

Without loss of generality, we can assume $\phi(\boldsymbol{k})$ to be a normalized wave function and β is an additional parameter controlling the total density. With the aid of the wave function ϕ, one can construct the exciton creation and destruction operators

$$\hat{B}^\dagger = \sum_{\boldsymbol{k}} \phi(\boldsymbol{k})\hat{e}_{\boldsymbol{k}}^\dagger \hat{h}_{-\boldsymbol{k}}^\dagger, \tag{36}$$

$$\hat{B} = \sum_{\boldsymbol{k}} \phi(\boldsymbol{k})\hat{h}_{-\boldsymbol{k}}\hat{e}_{\boldsymbol{k}} \tag{37}$$

that generate the transformation $\hat{U}(\beta) = \exp(\beta\hat{B}^\dagger)$. Acting on the TB ground state, $\hat{U}$ creates a coherent exciton state:

$$|\Psi\rangle_{\mathrm{BCS}} = Ce^{\beta\hat{B}^\dagger}|\Psi\rangle_{\mathrm{TB}} \equiv \prod_{\boldsymbol{k}}(u_{\boldsymbol{k}} + v_{\boldsymbol{k}}\hat{h}_{-\boldsymbol{k}}^\dagger\hat{e}_{\boldsymbol{k}}^\dagger)|\Psi\rangle_{\mathrm{TB}}, \tag{38}$$

reproducing the expectation values (34) and (35). Here, the normalization constant is $C = \exp[-1/2\sum_{\boldsymbol{k}} \ln(1 + \beta^2\phi^2(\boldsymbol{k})]$. The coherent excitonic state is equivalent to the BCS state with $u_{\boldsymbol{k}} = 1/\sqrt{1 + \beta^2\phi^2(\boldsymbol{k})}$ and $v_{\boldsymbol{k}} = \beta\phi(\boldsymbol{k})/\sqrt{1 + \beta^2\phi^2(\boldsymbol{k})}$.

As any Hartree-Fock state is uniquely determined by the expectation value of the basic single-particle operators, Eq. (38) represents the ground state if we identify $\beta\phi(\boldsymbol{k}) = f_{\boldsymbol{k}}/P_{\boldsymbol{k}}$ for any nontrivial solution of the gap equation and fix β by normalizing ϕ. At low densities, the commutator

$$[\hat{B}, \hat{B}^\dagger] = \sum_{\boldsymbol{k}} \phi^2(\boldsymbol{k})(1 - \hat{e}_{\boldsymbol{k}}^\dagger\hat{e}_{\boldsymbol{k}} - \hat{h}_{-\boldsymbol{k}}^\dagger\hat{h}_{-\boldsymbol{k}}) \tag{39}$$

is quasi-Bosonic and the exciton state is formally equivalent to a coherent Glauber state in quantum optics.

Clearly, for any fixed set $\{\phi(\boldsymbol{k})\}$, the total particle density is a monotonously increasing function of β and the tight-binding ground state with $\bar{P}_{\boldsymbol{k}} = \bar{f}_{\boldsymbol{k}} = \langle\hat{H}\rangle_{\mathrm{HF}} = 0$ corresponds to $\beta = 0$. For small β, the lowest-order contribution to the total energy is given by

$$E(\beta) = \beta^2\left[2\sum_{\boldsymbol{k}} \epsilon_{\boldsymbol{k}}\phi(\boldsymbol{k})^2 - \sum_{\boldsymbol{k}\boldsymbol{k}'} \phi(\boldsymbol{k})V(\boldsymbol{k}-\boldsymbol{k}')\phi(\boldsymbol{k}')\right] + \mathcal{O}(\beta^4). \tag{40}$$

Subsequent variation of $E/\beta^2 - \mu\sum_{\boldsymbol{k}}\phi(\boldsymbol{k})^2$ yields the linear Wannier equation for the wave function ϕ with eigenvalue μ. In the limit of vanishing density, the system energy is $E = \beta^2\mu = N\mu$, where $N = \beta^2$ is the total number of pairs in the low-density limit. Hence, if the linear Wannier equation allows for bound-state solutions with $\mu < 0$, the system can gain energy by forming bound e-h-pair states and a nontrivial solution of the gap equation is expected to exist.

In Ref. 32, bound exciton solutions are reported for parameter conditions corresponding to the regime of strong Coulomb interaction. These solutions vanish as the system transitions into a weakly interacting regime where the graphene fine-structure constant $\alpha_{\mathrm{G}} \lesssim 1/2$. To demonstrate the properties of the excitonic transformation (38), we take the wave function $\phi(\boldsymbol{k})$ obtained as numerical solution of the Wannier equation, and evaluate the energy of the state (38) for different values of β. For $\alpha_{\mathrm{G}} = 2.4$, which corresponds to the coupling strength in vacuum for vanishing dynamical screening, the result is shown in the left part of Fig. 5. Increasing β increases the number of

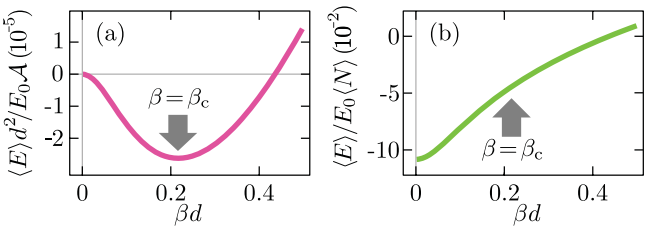

FIG. 5. (Color online) Results from evaluating the energy (a) and the energy per particle (b) for the state (38) for different values of β with a fixed wave function $\phi(\boldsymbol{k})$.

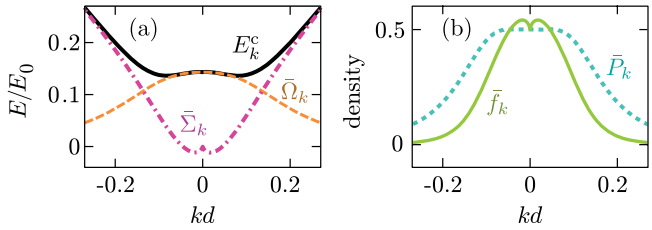

FIG. 6. (Color online) Numerical solutions of the gap equations, Eqs. (32) and (33) for $\alpha_G = 2.4$. (a) Ground-state Rabi energy $\bar{\Omega}$ (dashed line), ground-state renormalized energy $\bar{\Sigma}$ (dash-dotted line), and $E^c = (\bar{\Omega}^2 + \bar{\Sigma}^2)^{1/2}$ (solid line), all vs kd. Energies are given in units of $E_0 = \hbar v_F/d$. (b) Ground-state population $\bar{f}$ (solid line) and polarization $\bar{P}$ (dotted line) vs kd. These are related to the energies in (a) via Eqs. (30) and (31). Note how both $\bar{f}$ and $\bar{P}$ go to 1/2 at $k = 0$, and that the region where $\bar{f} > 1/2$ corresponds to the region where $\bar{\Sigma} < 0$.

pairs contributing to an energy reduction while simultaneously the energy gain per pair [see Fig. 5(b)] decreases due to the Pauli blocking. As a result, the obtained energy function has a clear minimum at $\beta_c d \approx 0.2$. We can also note that this minimum is clearly below the energy at $\beta = 0$. The energy per pair [see Fig. 5(b)] at $\beta = \beta_c$ is approximately one half of the exciton binding energy $\langle E\rangle/\langle N\rangle|_{\beta=0}$.

As any nontrivial solution of the gap equation produces a wave function via $\beta\phi(\boldsymbol{k}) = f_k/P_k$, solving the gap equation is equivalent to the minimization of the ground-state energy with respect to the full set $\beta\phi(\boldsymbol{k})$ and must yield better results than variation with respect to the single variational parameter β. Hence, the existence of bound-state solutions of the linear Wannier equation is an unambiguous sign for a nontrivial solution of the gap equation.

The solution of the gap equation defines the mean-field Hamiltonian

$$\hat{H}^{\mathrm{MF}} = \sum_{\boldsymbol{k}} \bar{\Sigma}_{\boldsymbol{k}}(\hat{e}^\dagger_{\boldsymbol{k}}\hat{e}_{\boldsymbol{k}} + \hat{h}^\dagger_{-\boldsymbol{k}}\hat{h}_{-\boldsymbol{k}}) - \bar{\Omega}_{\boldsymbol{k}}(\hat{h}^\dagger_{-\boldsymbol{k}}\hat{e}^\dagger_{\boldsymbol{k}} + \hat{e}_{\boldsymbol{k}}\hat{h}_{-\boldsymbol{k}}) \quad (41)$$

with the single-particle dispersion

$$E^{c/v}_{\boldsymbol{k}} = \pm\sqrt{\bar{\Sigma}^2_{\boldsymbol{k}} + \bar{\Omega}^2_{\boldsymbol{k}}}. \quad (42)$$

The new valence band is below the TB valence band if either $\Omega_{\boldsymbol{k}} = 0$ and $\bar{\Sigma}_{k_F} = 0$ have a solution with positive Fermi wave number, in which case the new valence and conduction bands are degenerated at the Fermi level at $k = 0$ and $k = k_F$, or the gap equation has a nontrivial solution with $\bar{\Omega}_{\boldsymbol{k}} \neq 0$, for which the spectrum exhibits a gap of magnitude $2\bar{\Omega}_{\boldsymbol{k}=0}$ at the Dirac points. Obviously, or rather by construction, the BCS state is the ground state of the mean-field Hamiltonian, and the energy required to add a quasiparticle in the new conduction or valence band is given by $E^{c/v}_{\boldsymbol{k}}$ and that to create an e-h pair by $E^c_{\boldsymbol{k}} + E^v_{\boldsymbol{k}}$. Nevertheless, the density of states in the pseudogap is nonzero since the Bogoliubov state characterized by the order parameters $\{\bar{\Omega}_{\boldsymbol{k}}, \bar{\Sigma}_{\boldsymbol{k}}\}$ has a finite overlap to states with order parameters $\{\bar{\Omega}_{\boldsymbol{k}} + \delta\Omega_{\boldsymbol{k}}, \bar{\Sigma}_{\boldsymbol{k}} + \delta\Sigma_{\boldsymbol{k}}\}$. Hence, within the Bogoliubov basis, single-particle excitations are described by scattering within the pseudoparticle bands, while collective excitations of the many-body system lead to deformation of the bands that vary the system energy continuously through the pseudogap.

C. Numerical solution of the gap equations

Figure 6 shows the solution of the full gap equations for $\alpha_G = 2.4$. Numerically, we evaluated the gap equation iteratively, using the optimized excitonic state generated by the solution of the linear Wannier equation as initial guess. Convergence was obtained within less than ten steps. We checked the robustness of the numerical solution against the initial guess. Starting with different values of β requires only a few more iterations until convergence is reached but produces the same solution. Due to the form factor in the Coulomb matrix elements, all integrals are well behaved and no additional cutoff parameters are required to achieve convergence. Figure 6(a) shows the resulting internal field and the renormalized energies in units of $E_0 = \hbar v_F/d$.

We see that the full solution of the gap equation produces a large internal field, which decreases monotonously as a function of k. Overall, the renormalized energy deviates only slightly from the bare single-particle energy, which is due to the angle dependence of the Coulomb integrals. At $k = 0$, the renormalized energy starts at zero and for small positive k, it becomes slightly negative. In this region, $\bar{f}(k) > 1/2$, as can be seen from Fig. 6(b) showing the population and polarization distributions. At $k = 0$, both $\bar{f} = 1/2$ and $\bar{P} = 1/2$. Regarding the first derivative of the renormalized energy as renormalized Fermi velocity, our calculations do not confirm the logarithmic divergence predicted in Refs. 4 and 10 but instead, the Fermi velocity decreases and even becomes negative.

In Fig. 7, we show the internal field [see Fig. 7(a)] and renormalized energies [see Fig. 7(b)] for $\alpha_G = 0.9$, 1.0, 1.1, and 1.2. From the Wannier equation, we know that the exciton binding energy decreases rapidly with decreasing effective fine-structure constant, and from this, we expect a similar behavior for the internal field. Indeed, decreasing the coupling constant from 1.2 to 0.9 decreases the internal field about one order of magnitude, while the renormalized energies are hardly distinguishable from the bare single-particle energies. Under all conditions, the particle and polarization distribution at $k = 0$ are 1/2 see Figs. 7(c) and 7(d). With increasing wave number, the distributions fall off very rapidly and the integrated particle and polarization density decrease with decreasing α_G.

In Fig. 8, we show the total energy density [see Fig. 8(a)], energy gain per pair [see Fig. 8(b)], and pair density [see Fig. 8(c)] as functions of α_G. The energy gain per pair starts at zero for $\alpha_G \approx 1/2$ and increases rapidly with increasing α_G, yielding approximately 1.6 eV for $\alpha_G = 2.4$. Increasing

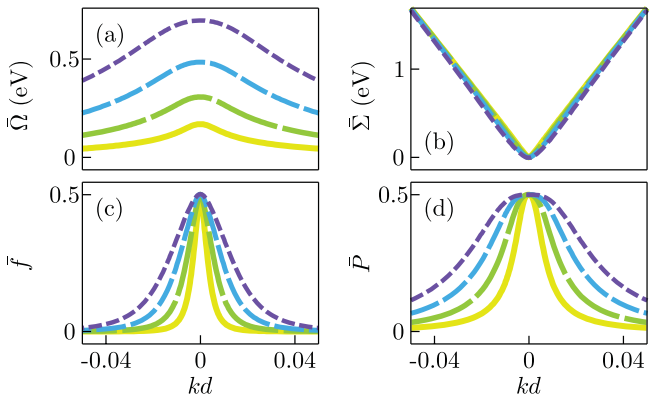

FIG. 7. (Color online) Solutions of the gap equation for different values of the fine-structure constant. Upper part: (a) ground-state Rabi energy $\bar{\Omega}$ and (b) renormalized single-particle energy $\bar{\Sigma}$ vs kd for $\alpha_G = 0.9$ (solid yellow line), 1.0 (long-dashed green line), 1.1 (medium-dashed blue line), and 1.2 (short-dashed purple line). The energy values have been obtained using $v_F = 9.07 \times 10^5$ and $d = 0.18$ Å. Lower part: population (c) and polarization (d) distributions.

α_G from .5 to 2.4 increases the total energy gain per cm^2 over approximately 20 orders of magnitude, which is a combined effect of the increasing energy gain per pair and the increasing pair density. At $\alpha_G = 2.41$, the pair density is $\langle N\rangle/\mathcal{A} = 2.16 \times 10^{14}$ cm^{-2}, which should be compared with the total density $n_0 = 1.27 \times 10^{15}$ cm^{-2} of the valence band electrons.

Figure 9 shows the resulting quasiparticle dispersion calculated from Eq. (42) for different values of the effective fine-structure constant in comparison with the noninteracting TB bands. The shaded dotted area shows the full tight-binding dispersion and the black dotted line the linear approximation to the TB dispersion, respectively. As can be recognized, deviations of the linear approximation from the full TB band structure can be neglected for energy ranges up to roughly 1 to 1.5 eV. For values of α_G exceeding the critical value $\alpha_c \approx 1/2$, a gap opens that increases rapidly with increasing α_G. As can be recognized, the band minima do not occur exactly at the

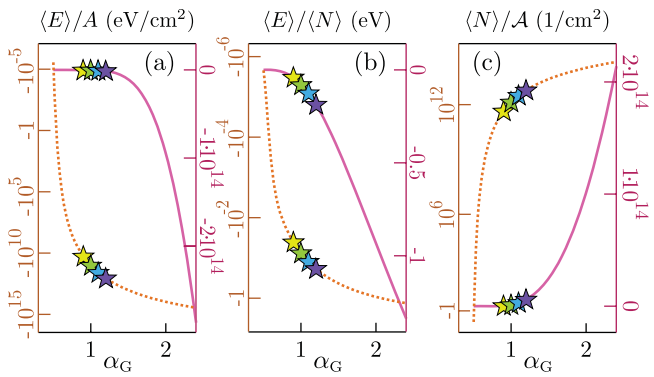

FIG. 8. (Color online) Energy density (a), energy gain per pair (b), and pair density (c) as functions of the coupling constant α_G. The dotted curves show the quantities on a logarithmic scale (left axis) and the solid curves present the same quantities on a linear scale (right axis). The stars correspond to the gap equations solutions in Fig. 7.

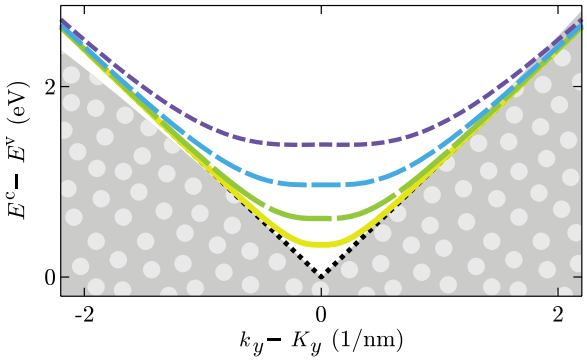

FIG. 9. (Color online) Dependence of the quasiparticle band structure $E^c_k - E^v_k$ [see Eq. (42)] on the effective fine-structure constant α_G. The curves shown are for $\alpha_G = 0.9$ (solid yellow line), 1.0 (long-dashed, green line), 1.1 (medium-dashed, blue line), and 1.2 (short-dashed, purple line), together with the linear TB dispersion (dotted black line). The shaded, dotted area shows the full TB dispersion. These band structures correspond to the gap-equations solutions in Fig. 7.

Dirac points but are slightly shifted toward finite k values. This is a result of the negative renormalized energy in the region where inversion occurs and is increasingly pronounced for large coupling strengths. For values of $\alpha_G \lesssim 1.1$, the Bogoliubov bands lie well within the validity range of the linear approximation to the TB bands. For higher values, corrections beyond the linear approximation should be taken into account, however, this is beyond the scope of this article.

IV. OPTICAL RESPONSE

To illustrate the influence of Coulomb effects on measurable quantities, we calculate the optical response of our graphene model system. For this purpose, we derive the graphene Bloch equations (GBE) and compute the linear response to an external optical field. In all calculations, the initial conditions will be chosen such that the graphene sheet is excited from the BCS ground state by a normally incident optical or terahertz pulse.

As shown in Sec. II, at normal incidence, the two degenerate Dirac points couple to the right and left circular polarized components of the transverse optical field. Hence, the circular polarization components provide a natural basis for the optical field in which the different polarizations are decoupled. Each polarization component of the vector potential obeys the wave equation

$$\Delta A^{\pm} - \frac{\epsilon}{c^2}\frac{\partial^2}{\partial t^2}A^{\pm} = -\frac{4\pi}{c}j^{\pm}. \tag{43}$$

Here, $j^{\pm} = -c\langle\frac{\delta H_I}{\delta A^{\pm *}}\rangle$ is the expectation value of the total current

$$\begin{aligned} j^{\pm} &= -\frac{e^2 n_0}{m_0 c}A^{\pm}(z=0,t)f(z) \\ &\quad + \frac{e|\boldsymbol{\pi}|}{m_0}\sum_{\boldsymbol{k}}[(1-2f_{\boldsymbol{k}})\cos\theta_{\boldsymbol{k}} \mp \mathrm{Im}(P_{\boldsymbol{k}})\sin\theta_{\boldsymbol{k}}]f(z) \\ &= -\frac{e^2 n_0}{m_0 c}A^{\pm}(z=0,t)f(z) + j^{\pm}_{[p]}f(z), \end{aligned} \tag{44}$$

with $f(z) = \int d^2\rho |\phi_{p_z}(\boldsymbol{r})|^2 \approx \delta(z)$ on the scale of the optical or terahertz wavelength. The total current consists of two contributions. The first is simply proportional to the vector potential and hence purely classical. Its only dependence on material quantities is via the charge density $\rho(\boldsymbol{r}) = -en_0 f(z)$, where n_0 is the total density of the electrons in the π band. This term is responsible for a Drude-like response. The second part of the current is purely particle-like and is associated with inter and intraband transitions. Due to the phase $\theta_{\boldsymbol{k}}$, isotropic electron and hole distributions or polarizations do not contribute to a macroscopic particle current. Hence, if the system is in its ground state and in the absence of external fields, there is no macroscopic current.

A. Graphene Bloch equations

To calculate the particle current, we divide the polarization and the particle distributions into a static part arising from the ground state, and a dynamical part arising from the optical excitations:

$$P_{\boldsymbol{k}} = \bar{P}_{\boldsymbol{k}} + \Delta P_{\boldsymbol{k}}, \tag{45}$$

$$f_{\boldsymbol{k}} = \bar{f}_{\boldsymbol{k}} + \Delta f_{\boldsymbol{k}}, \tag{46}$$

and, correspondingly, for the renormalized and Rabi energies. In a first approximation, all contributions beyond Hartree-Fock are treated phenomenologically by introducing constant dephasing and relaxation rates, i.e., $d\Delta P_{\boldsymbol{k}}/dt = -\gamma \Delta P_{\boldsymbol{k}}$ and similar for the populations. Noting that $\bar{P}_{\boldsymbol{k}}$ is real, the GBE for the dynamical part of the polarization and particle distribution are obtained as

$$\begin{aligned} i\hbar \frac{d}{dt}\Delta P_{\boldsymbol{k}} = {} & 2\big(\bar{\Sigma}_{\boldsymbol{k}} + \Delta\Sigma^r_{\boldsymbol{k}}\big)\Delta P_{\boldsymbol{k}} - (1 - 2\bar{f}_{\boldsymbol{k}} - 2\Delta f_{\boldsymbol{k}})\Delta\Omega^R_{\boldsymbol{k}} \\ & + 2\Delta\Sigma_{\boldsymbol{k}}(\bar{P}_{\boldsymbol{k}} + \Delta P_{\boldsymbol{k}}) + i(1 - 2\bar{f}_{\boldsymbol{k}} - 2\Delta f_{\boldsymbol{k}})\Delta\Omega_{\boldsymbol{k}} \\ & + 2\bar{P}_{\boldsymbol{k}}\Delta\Sigma^r_{\boldsymbol{k}} + 2\bar{\Omega}_{\boldsymbol{k}}\Delta f_{\boldsymbol{k}} - i\hbar\gamma\Delta P_{\boldsymbol{k}}, \end{aligned} \tag{47}$$

$$\begin{aligned} \hbar \frac{d}{dt}\Delta f_{\boldsymbol{k}} = {} & -2\,\mathrm{Im}\big(\Delta P^*_{\boldsymbol{k}}\Delta\Omega^R_{\boldsymbol{k}}\big) + 2\Delta\Omega_{\boldsymbol{k}}[\bar{P}_{\boldsymbol{k}} + \mathrm{Re}(\Delta P_{\boldsymbol{k}})] \\ & - 2\,\mathrm{Im}\big(\bar{P}_{\boldsymbol{k}}\Delta\Omega^R_{\boldsymbol{k}} + \bar{\Omega}_{\boldsymbol{k}}\Delta P^*_{\boldsymbol{k}}\big) - \hbar\gamma\Delta f_{\boldsymbol{k}}. \end{aligned} \tag{48}$$

In Eq. (47), the first line is the direct generalization of the familiar homogeneous part of the SBE, producing the generalized Wannier equation. The dynamical part of the Rabi energy, $\Delta\Omega^R_{\boldsymbol{k}}$, contains the optical field and the internal field of the optically induced interband polarization only, while both the ground-state and the dynamical populations contribute to the renormalization of the single-particle energies and the phase-space filling, reducing the effective Coulomb interaction. The second line describes an energy renormalization due to the optical field and Auger scattering proportional to $\Delta\Sigma_{\boldsymbol{k}}$, and Auger contributions proportional to $\Delta\Omega_{\boldsymbol{k}}$ that act as a source/drain for the dynamical polarization. These processes are very ineffective in a wide-gap semiconductor and are usually neglected in the SBE. The last line of Eq. (47) describes the coupling of the polarization to the populations via the ground-state polarizations. These contributions do not exist in the SBE and are specific for an excitonic ground state.

The first line in the equation of motion for the populations, Eq. (48), is the direct generalization of the SBE. The respective terms contain dynamical quantities only and are at least of second order in the optical field. The second line describes the conversion of polarizations into populations via Auger scattering processes proportional to $\Delta\Omega_{\boldsymbol{k}}$. The last line describes ground-state polarization assisted sources, specific for the excitonic ground state.

The major effect of the ground-state polarization is the introduction of a linear source for the optically induced populations $f_{\boldsymbol{k}}$. As a result, within a power expansion in terms of the exciting field, both the dynamical polarization and the population contain all powers of the exciting field. For any arbitrary order, the equations of motion are inherently coupled by the contributions proportional to $\bar{P}_{\boldsymbol{k}}$ in the last lines of Eqs. (47) and (48), and hence, must be solved simultaneously rather than iteratively. It is exactly this polarization-mediated coupling that is responsible for the occurrence of the Bogoliubov gap in the linear spectrum.

B. Linear optical spectra

To illustrate the basic effects of several contributions to the optical response, we solve the linearized GBE for a given external optical field. Examples of the results for $\alpha_{\mathrm{G}} = 2.4$ and $\hbar\gamma = 5 \times 10^{-4} E_0$ are shown in Fig. 10. The spectrum shows $4\pi\,\mathrm{Im}(j^{\pm}/\omega A^{\pm})$, which is a direct measure for the absorption. We notice pronounced excitonic resonances at low energies followed by a spectrally flat response. Due to the optical selection rules, all bright excitonic resonances have a p-like symmetry. Similar to the spectra in semiconductors, the peak height increases with increasing binding energy, showing that oscillator strength is transferred to strongly bound excitons.

Ignoring all Coulomb effects in the GBE, other than those responsible for the excitonic ground state, gives the artificial spectrum shown by the dashed (blue) curve in Fig. 10. This solution is equivalent to that obtained using only the mean-field Hamiltonian (41). The resulting spectrum is proportional to the

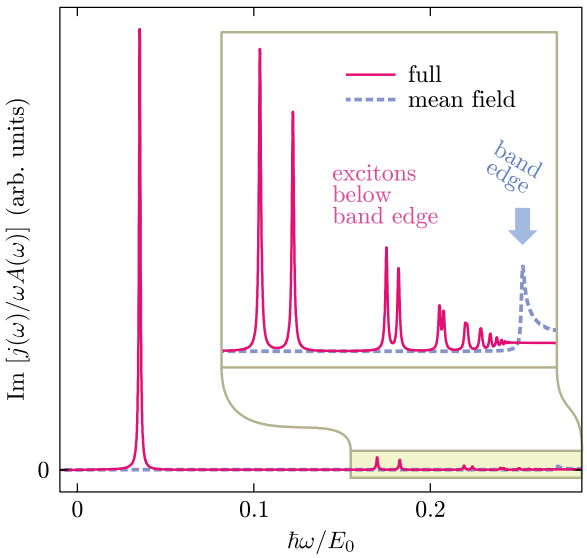

FIG. 10. (Color online) Imaginary part of the linear susceptibility for a graphene-like system with $\alpha_{\mathrm{G}} = 2.4$. Energy in units of $E_0 = \hbar v_F/d$.

density of states (DOS) (divided by ω) of the Bogoliubov bands and has no additional structure. The onset of the continuum absorption starts with a $1/\sqrt{\hbar\omega - E_G}$-like damped singularity exactly at the Bogoliubov gap. The origin of the singularity is the shift of the band minimum to finite k values (see Figs. 6 and 7). Within a quadratic approximation, $E(k) = E_G + \hbar^2(|k| - k_0)^2/2m_{\rm eff}$, the DOS

$$g(E) = \frac{m_{\rm eff}}{\pi\hbar^2}\theta(E - E_G)\left[1 + \sqrt{\frac{\hbar^2 k_0^2}{2m_{\rm eff}(E - E_G)}}\right],$$

consists of a steplike contribution typical for 2D parabolic bands and a singular part proportional to the shift k_0 that is similar to the free-particle result of a semiconductor quantum wire.[31] Energetically above the Bogoliubov gap, the optical response assumes the "universal" value given by $\frac{1}{2}\pi\alpha(e^*/e)^2$, where $\alpha = e^2/\hbar c$ is the fine-structure constant and $e^* = e|\boldsymbol{\pi}|/\sqrt{2}m_0 v_F$ is the effective charge, producing the effective medium Hamiltonian $H_0 + H_I^{[p]} = v_F\boldsymbol{\sigma}\cdot(\boldsymbol{p} - e^*/c\boldsymbol{A})$ where $\boldsymbol{\sigma} = (\sigma_x, \pm\sigma_y)$ combines the Pauli spin matrices. The effective charge depends on the optical matrix element and can either be calculated from the carbonic wave functions or be used as a fitting parameter. An additional factor two arises if the spin degeneracy is taken into account. Note that there is no valley degeneracy for the excitation with circularly polarized light.

Including all Coulomb interaction terms, we obtain several, clearly recognizable excitonic resonances below the pseudogap, shown by the solid (pink) curve in Fig. 10. The resonances arise from the Coulomb interaction of the optically induced excitations only, while the excitonic ground-state populations open the required gap.

To study the influence of dephasing, we repeated the calculation for the dephasing values in the range from $\hbar\gamma = 5\times10^{-4}E_0$ (lightest, most peaked curve) to $\hbar\gamma = 5\times10^{-2}E_0$ (darkest, flattest curve). As we can see in Fig. 11, the excitonic spectra broaden and the fine structure close to the gap smoothens to a flat, continuum-like response. The lowest exciton resonance is clearly recognizable for dephasing rates $\hbar\gamma$ up to $5\times10^{-3}E_0$.

To study the influence of the Auger contributions, we present in Fig. 12 results where we artificially vary the relative strength of the Auger terms between 0 (no Auger terms) and 1 (full Auger contributions). The comparison shows

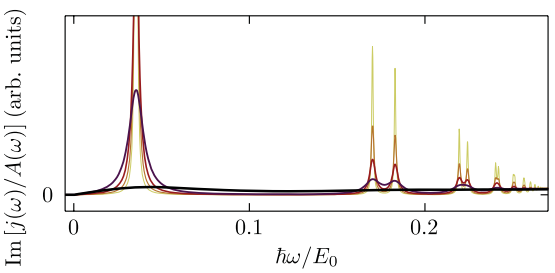

FIG. 11. (Color online) Effect of dephasing on the spectra of a graphene-like system with $\alpha_G = 2.4$. The curves show the results for dephasing constants (from most to least peaked) $\hbar\gamma/E_0 = 5\times10^{-4}$, 1×10^{-3}, 2×10^{-3}, 5×10^{-3}, and 5×10^{-2}. Energies in units of $E_0 = \hbar v_F/d$.

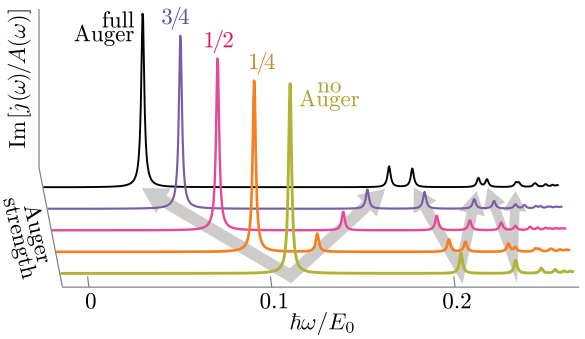

FIG. 12. (Color online) Imaginary part of the linear susceptibility for a graphene-like system with $\alpha_G = 2.4$. Energy in units of $E_0 = \hbar v_F/d$.

that the Auger contributions not only increase the exciton binding energy significantly, but they are also responsible for the splitting of the individual resonances. In the absence of the Auger contributions, the two distinct projection states of the angular momentum onto the propagation direction of the incident light are degenerated. As the Auger contributions invert the rotational symmetry they remove this degeneracy. The splitting of the resonances increases with increasing strength of the Auger terms and is symmetric with respect to the energy shift. The oscillator strength is distributed nonequally among the resonances. The curves in Fig. 12 show $\mathrm{Im}(j/A)$, which differs by a factor $1/\omega$ from the absorption spectra. This presentation shows that the heights of the absorption peaks vary like $1/\omega$ with a constant prefactor that is considerably larger for the lowest-lying state and independent of the strength of the Auger terms. As the Auger terms vanish for s-like states, the splitting confirms the p-like symmetry of the optically bright exciton resonances.

In Fig. 13, the absorption spectra for several values of the coupling strength and a fixed dephasing rate $\hbar\gamma = 13$ meV are shown. Variation of the effective coupling strength can be realized by embedding the graphene sheet in, or putting it on top of a dielectric medium, altering the static screening $\epsilon = \epsilon_r$ or $\epsilon = (1 + \epsilon_r)/2$, respectively. In the strong Coulombic regime with $\alpha_G \gtrsim 1/2$, all spectra show one clearly recognizable discrete absorption peak and a flat continuum response. Increasing the coupling strength results in a

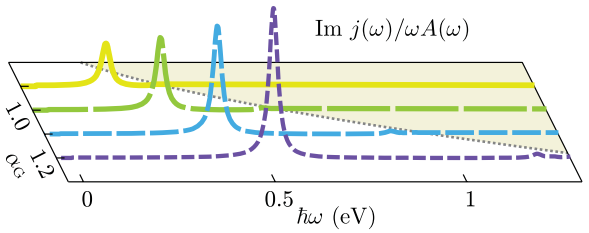

FIG. 13. (Color online) Imaginary part of the linear susceptibility for a graphene-like system for $\alpha_G = 0.9$ (solid yellow line), $\alpha_G = 1.0$ (long-dashed green line), $\alpha_G = 1.1$ (medium-dashed blue line) and $\alpha_G = 1.2$ (short-dashed purple line). The α_G-dependent energy gap (dotted line) marks the onset of the free-particle continuum (shaded area). These spectra correspond to the gap-equations solutions in Fig. 7 and to the band structures in Fig. 9.

significantly increased oscillator strength and a blueshift of the dominant absorption peak.

The blueshift of the excitonic resonance is in strong contrast to the expected behavior of an intrinsic direct-gap semiconductor, and is a clear signature of the excitonic ground state. In a conventional semiconductor quantum well (QW) system with a gap larger than the $1s$-exciton binding energy, the linear susceptibility is given by the Elliot formula

$$\chi^{\mathrm{QW}}(\omega) = -|d_{\mathrm{cv}}|^2 \sum_{\lambda} \left[\frac{|\psi_\lambda(r=0)|^2}{\hbar(\omega + i\gamma) - (E_g + E_\lambda)} - \frac{|\psi_\lambda(r=0)|^2}{\hbar(\omega + i\gamma) + (E_g + E_\lambda)} \right],$$

where d_{cv} is the dipole moment and E_λ and ψ_λ are the eigenvalues and eigenfunctions of the 2D hydrogenic Wannier equation, respectively. The resulting linear absorption $\propto \mathrm{Im}(\chi^{\mathrm{QW}})$ shows resonances at $\hbar\omega = E_g + E_\lambda$ with an oscillator strength $\propto |\psi_\lambda(r=0)|^2$. Hence, only s-like states contribute to the linear absorption of a QW system in contrast to the bright states with p-like symmetry in graphene. Defining the effective coupling strength as $\alpha_{\mathrm{eff}} = e^2/\epsilon\hbar c = \alpha/\epsilon$, in the strict 2D limit, the eigenvalues are proportional to the exciton energy unit $E_0 = \alpha_{\mathrm{eff}}^2 m_r c^2$ and $\psi_\lambda(r=0) \propto 1/a_0 = \alpha_{\mathrm{eff}}/\lambda_c$. Here, m_r is the reduced mass of the electron-hole pair, $\lambda_c = \hbar/(m_r c)$ is the corresponding Compton wavelength, and a_0 is the exciton Bohr radius, respectively. Hence, both the exciton binding energy and the oscillator strength scale quadratically with the coupling strength. As long as the band gap is independent of the background screening, the spectral position of the lowest exciton experiences a redshift proportional to α_{eff}^2.

Clearly, in graphene, the dependence on the effective coupling strength is much more complicated. As the occurrence of the excitonic resonances requires the opening of the gap, the coupling must exceed the critical value for the excitonic transition of the ground state. Once the coupling exceeds the critical value, both the exciton binding energy and oscillator strength increase with increasing coupling strength. Whereas stronger exciton binding and larger oscillator strength also appear in conventional semiconductors, in graphene, the simultaneous shift of the band edge toward higher energies results in the net *blueshift* of the lowest excitonic resonance, see Fig. 9, which is in strong contrast to the above discussed excitonic redshift in conventional semiconductors.

V. SUMMARY AND CONCLUSIONS

In conclusion, we presented a framework to determine the ground state and optical response of graphene and graphene-like systems. Our method is based on the equations of motion for the basic variables combined with a variational ansatz for the ground state. Even though we have only presented results on the singlet level, our method can be extended for a systematic and self-consistent inclusion of, for example, higher order many-body correlations or dynamical screening, treating the ground-state properties and excitation dynamics on equal footing. The presented theoretical scheme can be generalized to finite temperatures, adapted to other strongly correlated systems, or can include additional constraints like doping.

Within the Hartree-Fock approximation, our procedure produces the gap equations describing an excitonic ground state, including a renormalization of the single-particle energy. Similar equations without energy renormalization have been derived within a Dyson-Schwinger formalism,[8] and, including the single-particle energy renormalization, within a variational approach applied to an explicit excitonic wave function ansatz.[18–20] As has been discussed in Refs. 19 and 20, the instability of the TB ground state is closely related to the existence of bound-state solutions of the corresponding two-body problem. Indeed, we could relate the criterion for exciton condensation of the ground state with the existence of bound s-exciton solutions of the linear Wannier equation discussed in Ref. 32.

Our numerical analysis of the gap equations predicts an insulating ground state with gapped single-particle dispersion if the effective coupling constant $\alpha_{\mathrm{G}} \gtrsim 1/2$, which is in general agreement with other nonperturbative approaches studying the semimetal-to-insulator transition,[11,12,18–20] and with an analysis of the low-density graphene Wannier equation,[32] where a second-order phase transition from a weakly to a strongly Coulomb interacting regime was predicted. Our analysis fully includes finite-size effects arising from the carbonic atomic orbitals, yielding a well behaved transition into an excitonic ground state. This way, we evade any instability or need for ultraviolet cutoff parameters allowing us to determine the magnitude of the opened quasiparticle gap quantitatively, which is a precondition for an experimental verification.

On the basis of our approximation for the ground state, we derived the graphene Bloch equations for the strongly interacting regime on the singlet level. The self-consistent numerical solutions allow us to predict the optical response from the BCS ground state. Unlike in direct-gap semiconductors, where electron-hole recombinations are dipole allowed, s-like excitons in graphene are optically dark and hence radiatively stable, while bright excitons have p-like symmetry. As a hallmark of an excitonic ground state, the excitonic resonances undergo a blue shift if the effective coupling strength is increased, which can be achieved within a certain range by manipulation of the dielectric environment. Assuming a nominal coupling strength $\alpha_{\mathrm{G}} = 2.4$ for graphene in air, the effective coupling strength for graphene on a typical substrate like SiC or SiO_2 covered by air is $\alpha_{\mathrm{G}} \approx 0.53$ and $\alpha_{\mathrm{G}} \approx 1.08$, respectively. Additional fine-tuning can be achieved, e.g., by controllably depositing various layers of ice or oil on the graphene sheet.[39]

As intrinsic screening may alter the nominal value of the fine-structure constant,[16,40] it may turn out to be crucial for the realization of an excitonic ground state in graphene. Studies on the excitonic instability in graphene that include different screening models predict an increased value of the critical coupling constant depending on the model[20] used, still well below 2.4. However, to clarify this issue, screening must be included self-consistently with the evolving gapped quasiparticle dispersion, which is one of the topics of our ongoing studies. Other topics of future research are the inclusion of higher-order correlations, the inclusion of Coulomb scattering, and the extension to optical nonlinearities.

[1]K. S. Novoselov, A. K. Geim, S. V. Morozov, D. Jiang, Y. Zhang, S. V. Dubonos, I. V. Grigorieva, and A. A. Firsov, Science **306**, 666 (2004).
[2]F. Bonaccorso, Z. Sun, T. Hasan, and A. C. Ferrari, Nat. Photon. **4**, 611 (2010).
[3]P. R. Wallace, Phys. Rev. **71**, 622 (1947).
[4]J. González, F. Guinea, and M. A. H. Vozmediano, Phys. Rev. B **59**, R2474 (1999).
[5]D. E. Sheehy and J. Schmalian, Phys. Rev. Lett. **99**, 226803 (2007).
[6]L. Fritz, J. Schmalian, M. Müller, and S. Sachdev, Phys. Rev. B **78**, 085416 (2008).
[7]A. Sinner and K. Ziegler, Phys. Rev. B **82**, 165453 (2010).
[8]D. V. Khveshchenko, Phys. Rev. Lett. **87**, 246802 (2001).
[9]D. V. Khveshchenko and W. F. Shively, Phys. Rev. B **73**, 115104 (2006).
[10]V. Juričić, I. F. Herbut, and G. W. Semenoff, Phys. Rev. B **80**, 081405 (2009).
[11]J. E. Drut and T. A. Lähde, Phys. Rev. Lett. **102**, 026802 (2009).
[12]J. E. Drut and T. A. Lähde, Phys. Rev. B **79**, 165425 (2009).
[13]L. Yang, J. Deslippe, C.-H. Park, M. L. Cohen, and S. G. Louie, Phys. Rev. Lett. **103**, 186802 (2009).
[14]E. Malić, J. Maultzsch, S. Reich, and A. Knorr, Phys. Rev. B **82**, 035433 (2010).
[15]A. D. Güçlü, P. Potasz, and P. Hawrylak, Phys. Rev. B **82**, 155445 (2010).
[16]J. P. Reed, B. Uchoa, Y. I. Joe, Y. Gan, D. Casa, E. Fradkin, and P. Abbamonte, Science **330**, 805 (2010).
[17]J. Sabio, F. Sols, and F. Guinea, Phys. Rev. B **81**, 045428 (2010).
[18]J. Sabio, F. Sols, and F. Guinea, Phys. Rev. B **82**, 121413 (2010).
[19]O. V. Gamayun, E. V. Gorbar, and V. P. Gusynin, Phys. Rev. B **80**, 165429 (2009).
[20]O. V. Gamayun, E. V. Gorbar, and V. P. Gusynin, Phys. Rev. B **81**, 075429 (2010).
[21]J. Wang, H. A. Fertig, and G. Murthy, Phys. Rev. Lett. **104**, 186401 (2010).
[22]J. Wang, H. A. Fertig, G. Murthy, and L. Brey, Phys. Rev. B **83**, 035404 (2011).
[23]I. F. Herbut, Phys. Rev. Lett. **97**, 146401 (2006).
[24]I. F. Herbut, V. Juričić, and O. Vafek, Phys. Rev. Lett. **100**, 046403 (2008).
[25]A. V. Shytov, M. I. Katsnelson, and L. S. Levitov, Phys. Rev. Lett. **99**, 246802 (2007).
[26]V. M. Pereira, J. Nilsson, and A. H. Castro Neto, Phys. Rev. Lett. **99**, 166802 (2007).
[27]A. H. Castro Neto, Physics **2**, 30 (2009).
[28]K. F. Mak, J. Shan, and T. F. Heinz, Phys. Rev. Lett. **106**, 046401 (2011).
[29]D.-H. Chae, T. Utikal, S. Weisenburger, H. Giessen, K. V. Klitzing, M. Lippitz, and J. Smet, Nano Lett. **11**, 1379 (2011).
[30]E. Engel and R. N. Schmid, Phys. Rev. Lett. **103**, 036404 (2009).
[31]H. Haug and S. W. Koch, *Quantum Theory of the Optical and Electronic Properties of Semiconductors* (World Scientific, Singapore, 2009).
[32]J. H. Grönqvist, T. Stroucken, G. Berghäuser, and S. W. Koch, e-print arXiv:1107.5653 (unpublished).
[33]M. Kira and S. W. Koch, Prog. Quantum Electron. **30**, 155 (2006).
[34]M. Hirtschulz, F. Milde, E. Malić, S. Butscher, C. Thomsen, S. Reich, and A. Knorr, Phys. Rev. B **77**, 035403 (2008).
[35]J. H. Grönqvist, M. Hirtschulz, A. Knorr, and M. Lindberg, Phys. Rev. B **81**, 035414 (2010).
[36]Inclusion of next-nearest-neighbor hopping into the TB Hamiltonian results in an energy shift of the Dirac points and a breaking of the electron-hole symmetry. The shift of the Dirac energy can be included into the definition of the Fermi level and does not alter the physics quantitatively. The breaking of the electron-hole symmetry is $O(\boldsymbol{k}^2)$ and can be neglected within the linear approximation.
[37]T. Stroucken, A. Knorr, P. Thomas, and S. W. Koch, Phys. Rev. B **53**, 2026 (1996).
[38]T. Meier, P. Thomas, and S. W. Koch, *Coherent Semiconductor Optics* (Springer-Verlag, Berlin, 2007).
[39]C. Jang, S. Adam, J.-H. Chen, E. D. Williams, S. Das Sarma, and M. S. Fuhrer, Phys. Rev. Lett. **101**, 146805 (2008).
[40]E. H. Hwang and S. Das Sarma, Phys. Rev. B **75**, 205418 (2007).